POLYMERS AND COLLOIDS

PETER SCHURTENBERGER
Institut für Polymere, ETH Zürich,
CH-8092 Zürich, Switzerland

ABSTRACT

A wealth of structural information from colloid and polymer solutions on a large range of length scales can be obtained using small angle neutron scattering (SANS) experiments. After a general introduction to the field of soft condensed matter, I shall give a few selected examples on how SANS combined with suitable contrast variation schemes can be used to extract information on the size and conformation of polymer coils in solution and in the melt, and on the local structure and flexibility of polymerlike micelles and microemulsions.

1. Introduction

During the last 10 - 20 years colloid and polymer sciences have undergone a 'renaissance', which has not only manifested itself in the creation of a new name, the term 'soft condensed matter', but indeed resulted in a considerable gain of understanding of the structural and dynamic properties of these complex fluids. The reason for this progress was on the one hand the realization of the existence of close analogies to established areas in theoretical physics such as between polymers and magnetic systems or field theory, or between colloidal suspensions and simple liquids. On the other hand, the availability of new experimental techniques such as dynamic light scattering or neutron scattering has also been instrumental in this development.

When talking about soft condensed matter, we generally consider three different areas: polymers, colloids and so-called association colloids or surfactant systems (see Fig. 1). Polymer sciences has greatly advanced in particular through the work of P. G. de Gennes, who for example demonstrated the existence of universal behavior (expressed through so-called scaling laws) for different physical properties of polymer solutions and melts. In such a treatment, the basic idea is to concentrate on global properties, i.e. on the dependence of observable physical properties such as the overall coil dimension (characterized for example by its radius of gyration, R_g) on chain length, concentration or a few basic interaction parameters, and reduce the polymer molecule to an idealized model omitting all chemical details. A classical model for such a description is the random walk with N completely independent steps as the simplest idealization of a flexible polymer chain consisting of N monomers in solution or in a melt. This simple model does in fact provide a very good description of the conformation of flexible polymer chains in theta solvents (where the different contributions to long range interactions between segments cancel and the polymer solution exhibits a pseudo-ideal behavior analogous to the Boyle point of gases) or melts. Additionally, one can for example take into account interactions between

neighbouring monomers (i.e., include the local 'chemistry') as done in the wormlike chain model, or include excluded volume interactions by modelling the polymer chain as a self-avoiding random walk.[1-3] SANS can then be used as a very good test of the predictions from the various theoretical models in order to assess their validity under various experimental conditions as will be demonstrated in the second chapter of this presentation.

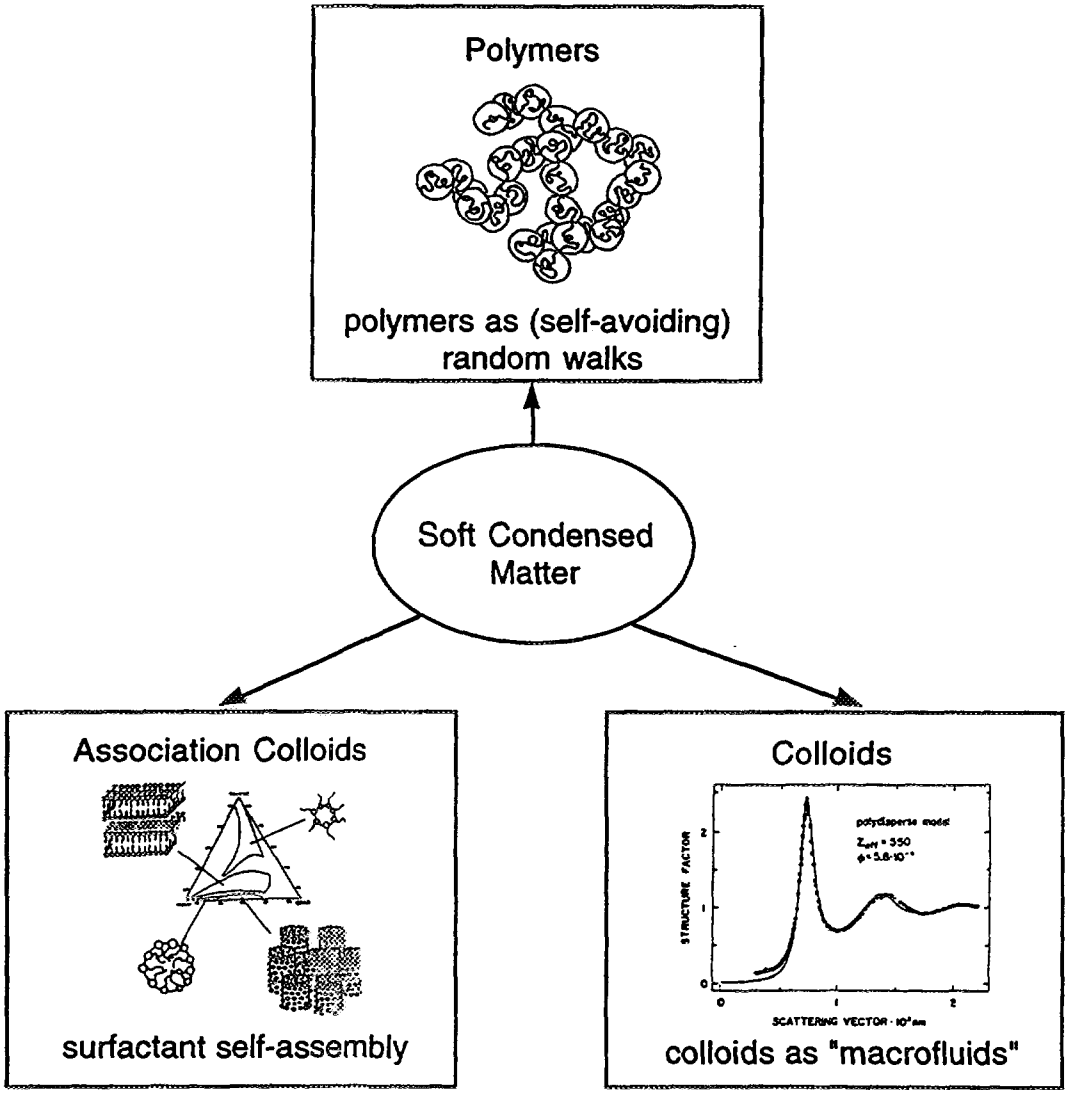

Fig. 1: An overview over some important areas in soft condensed matter

In colloidal suspensions, considerable progress in the understanding of questions such as the effect of interparticle interactions on the structure and stability of colloidal suspensions has been achieved by making analogies to simple fluids such as liquid argon. The idea is to make a typical coarse graining ansatz and consider a collection of colloidal particles as a 'macrofluid' dispersed in a continuous medium, i.e., the solvent is treated as a quasi-inert continuum that is defined through its macroscopic properties such as density, index of refraction and dielectric constant only. One can then apply the well known tools from statistical mechanics derived for simple liquids in order to create

a link between the suspension structure and the interaction potential.[4, 5] In this respect it is important to realize that the potential used as an input in the statistical mechanical treatment is a 'potential of mean force', and that the osmotic pressure now plays the role of the pressure in the corresponding atomic or molecular systems. SANS offers a very valuable tool to test these theoretical models and to obtain information on interparticle interactions and suspension structure.[4, 5]

Surfactants in solution exhibit a complex aggregation behavior as a result of a delicate balance of opposing forces.[6] An important aspect of surfactant systems is the relation between microstructure and phase equilibria. Several theoretical concepts based either on packing considerations of the surfactants in the aggregates or on the role of the bending elastic energy of the surfactant monolayer have provided us with a theoretical framework for a better understanding of these systems.[6, 7] In particular the 'flexible surface model', which is an interfacial description using curvature elasticity, has considerably advanced our understanding of many aspects of the complex phase behavior exhibited by surfactant systems.[7, 8] In these systems, SANS is a particularly powerful technique for determining structural properties on all length scales as it allows to specifically label certain components through contrast variation as will be demonstrated in chapter 3.

2. SANS from Polymer Solutions

In this chapter I shall discuss some structural aspects of linear polymers. As a classical example of such a polymer we can look at polystyrene:

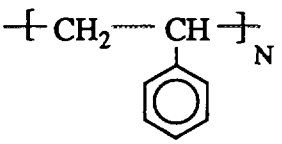

where the number of repeat (or monomer) units, N, which is often called the degree of polymerization, can be as large as > 10^6. As already mentioned, the simplest possible

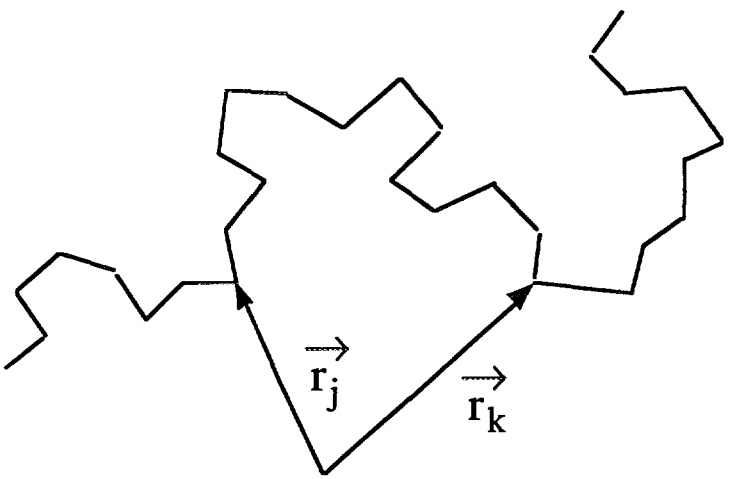

Fig. 2: Schematic representation of a random walk model of a linear polymer chain

model for the conformation of such a linear chain in solution is a random walk in three dimensions as shown schematically in Fig. 2.. The corresponding orientationally

averaged and normalized single particle scattering function P(Q), which contains all the structural information on the conformation of the scattering object can then be calculated according to

$$P(Q) = \frac{1}{N^2} \sum_{j=1}^{N} \sum_{k=1}^{N} \left\langle \frac{\sin(Qr_{jk})}{Qr_{jk}} \right\rangle \qquad (1)$$

where $r_{jk} = |\mathbf{r}_j - \mathbf{r}_k|$ is the distance between two scattering centres (monomers) and $\mathbf{Q}$ is the scattering vector. For the random walk model, the evaluation of Eq. 1 is particularly simple due to the Gaussian distribution for the intersegmental distances and leads to the so-called Debye function

$$P(Q) = \frac{2(e^{-x} + x - 1)}{x^2} \qquad (2)$$

where $x = \langle R_g^2 \rangle Q^2$ and $\langle R_g^2 \rangle$ is the mean square radius of gyration of the polymer coil. The Debye function results in the classical asymptotic behavior of $P(Q) \sim Q^{-2}$ for large values of x, which is the typical 'finger print' of a structure generated by a random walk. However, the local flexibility of polymer chains is basically caused by the potential energy of rotation about chemical bonds. While the random walk model assumes that the directions of individual chain segments are completely uncorrelated, i.e., that these rotations are completely unhindered, for 'real' polymers this is generally not true due to steric hindrances between side groups. Therefore, real chains are locally stiff, and it is only after a certain distance b (the Kuhn length or statistical segment length) along the chain that the direction of individual chain segments become completely uncorrelated and that the time averaged distance distribution function between two monomer units loses its local character and starts to obey Gaussian statistics. Furthermore, due to excluded volume effects between monomers we can expect that the ideal random walk model doe's not provide an adequate description of the stain statistics in good solvents, and that we have to use a self-avoiding random walk instead. This does not lead to Gaussian statistics for the distribution function of intersegmental distances and therefore does not allow for an easy evaluation of Eq. 1. Summarizing this short introduction to polymer statistics, we can point out the following characteristic features that we expect to find in data from scattering experiments with large single polymer coils in solution that cover a broad range of scattering vectors:

The data reveal a series of different regimes with a behavior characteristic of the various length scales of the chains: For very low values of Q ($1/Q < R_g$), i.e., in the so-called Guinier regime, the scattered intensity I(Q) becomes insensitive to structural details and is dominated by the finite overall length of the particles, and we can determine the radius of gyration R_g of the particles. At intermediate Q (cross section radius $R_c << 1/Q << R_g$), I(Q) becomes much more sensitive to the local aggregate structure, and polymer theory predicts for flexible polymer coils that I(Q) should decay with a power law of the form $I(Q) \sim Q^{-x}$, where x = 1.66 for a self-avoiding random walk chain and x = 2.0 for an ideal random walk chain. At large values of Q, I(Q) is controlled by distances over which polymers are rod-like rather than flexible, and we expect a crossover to an asymptotic Q^{-1}-dependence for I(Q) which is typical for locally cylindrical structures. However, a real polymer is not an infinitely thin chain, and therefore the local cross section structure of the chains give rise to a cross section Guinier behavior and a strong decrease in the scattering intensity at still larger Q-values. The different characteristic regimes are demonstrated in Fig. 3.

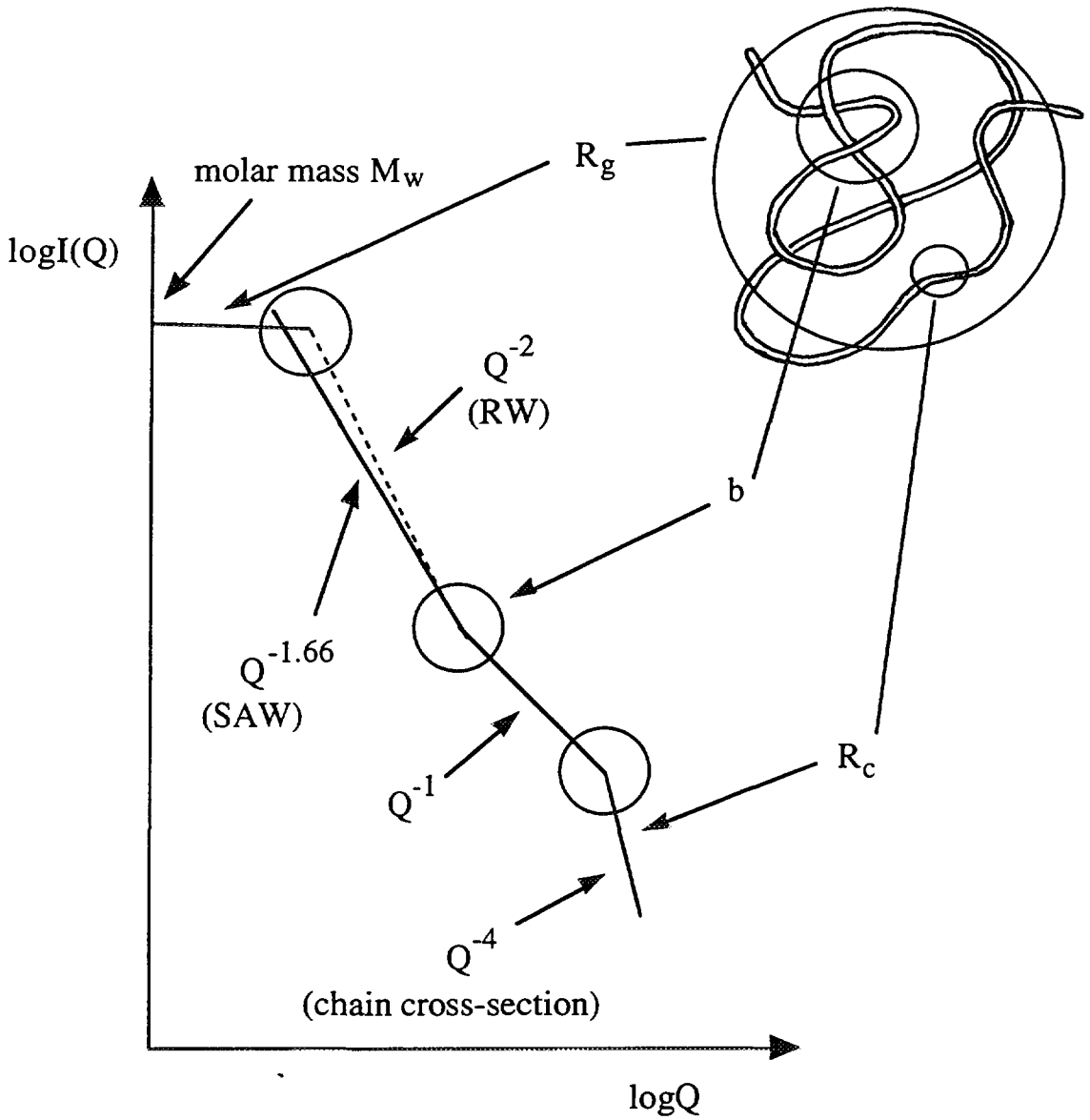

Fig. 3: Schematic plot of the asymptotic behavior of the scattering intensity I(Q) versus scattering vector Q for polymers in solution. The crossover regions are denoted by circles (see text for details).

However, it is important to point out that the experimental verification of the asymptotic behavior can be quite difficult, and in particular the crossover from a flexible to a locally stiff chain that contains the very important information on the polymer flexibility is often masked by the local cross section structure. This can be demonstrated with data from partially deuterated polymer chains, where different parts of the monomer unit contribute differently to the overall intensity. The scattering functions of atactic polystyrene (PS) in carbon disulfide (CS_2) with different selective deuteration of the polymer have been determined by Rawiso et al. [9] using SANS. CS_2 is a good solvent for PS, and this is reflected in the scattering function which shows a $Q^{-1.7}$-behavior at intermediate Q values. The data for a molar mass of $M_w \approx 50'000$ and three different selective deuterations ((i) fully deuterated, (ii) deuterated in the phenyl ring, and (iii) deuterated in the backbone) are shown in Fig. 4. CS_2 has a low scattering length density, C and D have a relatively large scattering length, and H has a negative

scattering length. Therefore it is mainly the deuterated parts of PS which contribute to the scattering from the polymer coil.

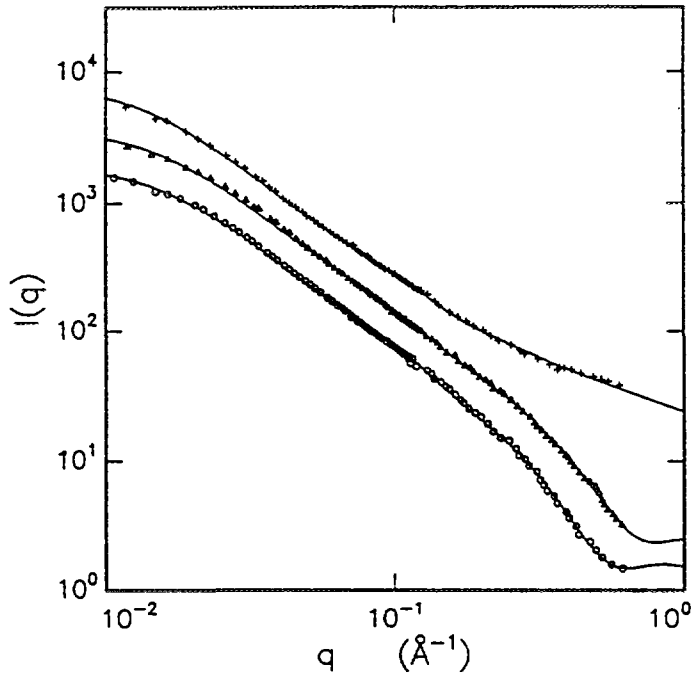

Fig. 4: Scattering functions for PS ($M_w \approx 50'000$) in CS_2.[9] The lower data are for fully deuterated PS, the middle data for the phenyl ring and the upper data for the backbone deuterated. The curves are fits for a model scattering function that includes excluded volume effects.[10]

At low Q values we observe a well defined Guinier regime from which we can determine the molar mass (or contour length L) as well as the radius of gyration. However, we also immediately see from Fig. 4 that both for the fully deuterated as well as the phenyl ring deuterated samples the relatively large cross section radius of the chain leads to a direct cross-over from the asymptotic $Q^{-1.7}$-behavior at intermediate Q values to the exponential decay in the cross section Guinier regime, thus completely masking the cross-over to the Q^{-1}-regime from which the Kuhn length b as a measure of the chain flexibility could be determined. It is only for the backbone deuterated sample, where the cross section radius is much smaller, that one is able to observe this part of the scattering function. In the original paper of Rawiso et al. the authors concentrated on the different asymptotic regimes in order to extract the maximum amount of data on the structure of PS in good solvents on all length scales, and no attempts were made to fit the data in the full Q range as the appropriate scattering functions for wormlike chains with excluded volume effects were not available. As a result of this unsatisfactory situation we started a series of off-lattice Monte Carlo simulations on semi-flexible polymer chains with and without excluded volume interactions.[11] The primary goal has been to obtain "experimental" data for the scattering function P(Q) for semi-flexible chains with excluded volume effects with an accuracy of about 1 % in the range up to Qb = 10 and to parameterize them in such a way that they can be used for model fitting of experimental scattering data on polymer-like micelles. The model used is a discrete representation of the worm-like chain model of Kratky and Porod. The parameters of a

chain are the contour length L, and the statistical segment length b. In practice the chain is represented by N points along the contour, such that L = Na, where a is the point separation ("bond length"). For the excluded volume effects the finite cross section radius of the micelle was taken into account by placing hard spheres of radius R = 0.1b at each point along the chain. Simulations were performed for chains with contour lengths of L/b = 0.3, 0.6, 1.25, 2.5, 5, 10, 20, 40, 80, 160, 320, and 640. The accuracy of the resulting P(Q) was estimated to be better than 1-2 % for L/b ≤ 160 and 2-3 % for L/b=320 and 640. The resulting P(Q) have been parameterized using various methods in order to obtain numerical approximations that can be used in the analysis of "real" experimental data. The most accurate (and general) method used follows an approach used by Yoshizaki and Yamakawa in order to obtain P(Q) for helical wormlike chains.[12] In this approach the scattering function can be written as

$$I(Q) = C_w \Delta\rho_m^2 S_{wc}(Q) S_c(Q) \langle M \rangle_w \qquad (3)$$

where C_w is the polymer concentration (in weight per volume), $\Delta\rho_m$ is the average excess scattering length density per unit mass, $S_{wc}(Q)$ and $S_c(Q)$ are the normalized scattering functions of the infinitely thin wormlike chains and of the cross section, respectively, and $\langle M \rangle_w$ is the weight average molar mass. The scattering function $S_{wc}(Q)$ is given by

$$S_{wc}(Q, L, b) = [(1 - \chi(Q, L, b))S_{chain}(Q, L, b) + \chi(Q, L, b)S_{rod}(Q, L)]\Gamma(Q, L, b) \quad (4)$$

where $S_{chain}(Q, L, b)$ is the scattering function of a flexible chain with excluded volume effect,[13] $S_{rod}(Q, L)$ is the scattering function of a stiff rod,[14] $\chi(Q, L, b)$ is a cross-over function and $\Gamma(Q, L, b)$ corrects the crossover region. Explicit expressions for $\chi(Q, L, b)$ and $\Gamma(Q, L, b)$ are given elsewhere.[10] Such a scattering function indeed allows for a quantitative analysis of scattering data form semi-flexible chains over a broad Q-range as can be verified with the data from polystyrene in a good solvent shown in Fig. 4. A fit of Eqs. 3 and 4 to the experimental data is shown in Fig. 4. In the fit the local cross section structure of PS was approximated by a cylindrical shape, for which the corresponding cross section scattering function can be written as

$$S_c(Q) = \left(\frac{2J_1(R_cQ)}{(R_cQ)} \right)^2 \qquad (5)$$

where $J_1(x)$ is the first order Bessel function and R_c the cross section radius.

The model scattering functions give almost perfect fits to the data over the entire range of Q values. The resulting values of the contour lengths L are in very good agreement with the calculated values based on the known molar mass and polydispersity for the three different samples. The Kuhn length is determined to be b = 24.8 Å, in good agreement with previous studies. The values for the cross-section radii that come out of the fit are also quite reasonable considering the molecular structure of the PS chain in solution as determined by other investigations. This clearly demonstrates that Eqs. 3 and 4 provide us with an analytical expression for the scattering cross section of polymers in good solvents capable of quantitatively reproducing the experimental features over an extended range of scattering vectors. This represents a major improvement compared to the previous characterization of

semiflexible polymers with small-angle scattering methods, where the analysis primarily relied on an individual interpretation of different Q-regimes based on asymptotic expressions. It also demonstrates the strength of SANS in the analysis of structural properties of polymers in solution, in particular when combined with contrast variation experiments and suitable model fits.

3. SANS from Polymerlike Micelles and Microemulsions

As pointed out in the introduction, surfactants in solution exhibit a complex aggregation behaviour as a result of a delicate balance of opposing forces.[6] Micellar solutions and microemulsions represent thermodynamically stable liquid dispersions containing surfactant aggregates, which can often be found in a large region of the phase diagram of 2- or multi-component surfactant systems.[15-17] In micellar dispersions, the aggregates are formed by self-assembly of surfactant monomers. While micelles are frequently spherical, they can also exhibit a sphere-to-rod transition and even grow to giant flexible and polymer-like aggregates. This micellar growth can be induced by a reduction in the so-called spontaneous curvature H_0 due to a change in a "control parameter" such as temperature (in nonionic surfactant systems), ionic strength (in ionic surfactant systems) or cosurfactant concentration, which subsequently results in a characteristic transition in the particle morphology from spheres to cylinders to lamellae.[8, 18, 19] Microemulsions are formed in 3- or multicomponent systems. The microemulsion aggregates have a liquid core (oil in oil-in-water (o/w), water in water-in-oil (w/o) microemulsions) which is surrounded and stabilized by a surfactant monolayer. They frequently possess a droplet-like structure, but they can also grow into large tubular or sponge-like and multi-connected structures.[8, 15] In addition to micellar and microemulsion phases, a number of liquid crystalline phases such as the lamellar (L_α), hexagonal (H) or cubic (I) phases or the so-called "sponge" phase (L_3) can be found.

A typical example for the phase behaviour of a ternary system with a nonionic surfactant of the ethylene oxide type is shown in Fig. 5. The surfactant-to-oil ratio is kept constant, and the temperature and the composition (characterized by the weight fraction of surfactant and oil) is allowed to vary, i.e., the system corresponds to a section through the phase prism as illustrated in Fig. 5(a). Three separate phases can be identified in the phase diagram shown in Fig. 5(b): A microemulsion phase, L, a lamellar liquid crystalline phase, L_α, and a second liquid phase, the so-called sponge or L_3 phase.[20] The relation between microstructure and phase equilibria is an important aspect of surfactant systems. Several theoretical concepts based either on packing considerations of the surfactants in the aggregates or on the role of the bending elastic energy of the surfactant monolayer have provided us with a theoretical framework for a better understanding of these systems.[6, 8, 21, 22] The sequence of phase transitions shown in Fig. 5(b) is, for example, in good agreement with the predictions of the flexible surface model.[8, 20] The phase transitions follow the trend of a decreasing mean curvature of the surfactant film with increasing temperature, i.e., are consistent with the strong temperature-induced variation of the spontaneous curvature for nonionic surfactants.[23] This temperature-induced variation of H_0 not only results in the appearance of phase transitions. It also causes variations of the microemulsion structure in the L-phase from almost monodisperse droplets at the lower phase boundary (the so-

called emulsification failure[8]) to anisotropic and possibly multiply-connected particles at the upper phase boundary.[20, 24, 25]

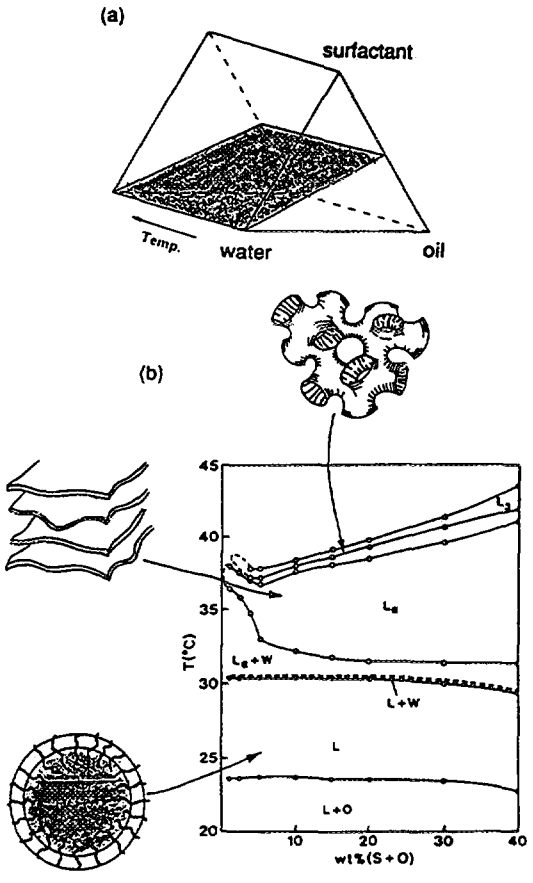

Fig. 5: (a) An illustration of the phase prism of a ternary system surfactant-water-oil. The shadowed region represents a plane through the phase prism defined by a constant surfactant-to-oil ratio (51.9/48.1 by weight). (b) Phase diagram of the system $C_{12}E_5$-D_2O-decane for a constant surfactant-to-oil ratio of 51.9/48.1 (see (a)), where temperature is plotted versus the total weight fraction of surfactant and oil. L denotes a liquid microemulsion phase, L_α is a lamellar liquid crystalline phase, and L_3 is an isotropic liquid phase often referred to as the "sponge phase" (adapted from ref. [8]).

It is this particular feature of micelles and microemulsions that makes scattering investigations of these systems so challenging. The micellar shape, the size distribution and the intermicellar interactions may depend strongly upon solution composition (e.g., surfactant concentration, ionic strength) and temperature, in contrast to other classical macromolecular systems such as polymers, biopolymers or lyophobic colloids. Therefore single particle properties such as the weight average molar mass M_w or the z-average mean square radius of gyration $\langle R_g^2 \rangle_z$ cannot be determined unambiguously from an extrapolation of the scattering data to infinite dilution. The neglect of this inherent property of surfactant systems and the various attempts to decouple micellar growth and intermicellar interactions have led to a number of controversies.

In the following paragraph I shall demonstrate that SANS can indeed provide important contributions to a better characterization of micellar structures in solution. It has been demonstrated in various reports that it is possible to find conditions where micelles or microemulsion particles grow dramatically with increasing surfactant concentration into giant cylindrical aggregates. These giant micelles normally have a high degree of flexibility, and their overall structure is generally well described by polymer theory.[18, 26] Several attempts have been made to demonstrate the existence of cylindrical micelles and to characterize the micellar structure using small-angle scattering experiments.[19, 27-34] The basis for such an approach comes from the fact that scattering experiments on polymers or polymer-like micelles covering a broad range of scattering vectors reveal a series of different regimes with a behavior characteristic of the various length scales of the chains as outlined in the previous paragraph (Fig. 3) These different characteristic regimes are indeed also found in solutions of polymerlike micelles as demonstrated in Fig. 6 with data form polymer-like lecithin reverse micelles, where results from static light and small-angle neutron scattering experiments have been combined. The particular example used is a microemulsion system in which giant polymerlike and tubular aggregates form. This formation of polymer-like structures upon the addition of trace amounts of water to almost spherical lecithin reverse micelles in organic solvents such as isooctane or cyclohexane has been demonstrated with a combination of light scattering and small-angle neutron scattering at low surfactant concentrations, which allowed verification of

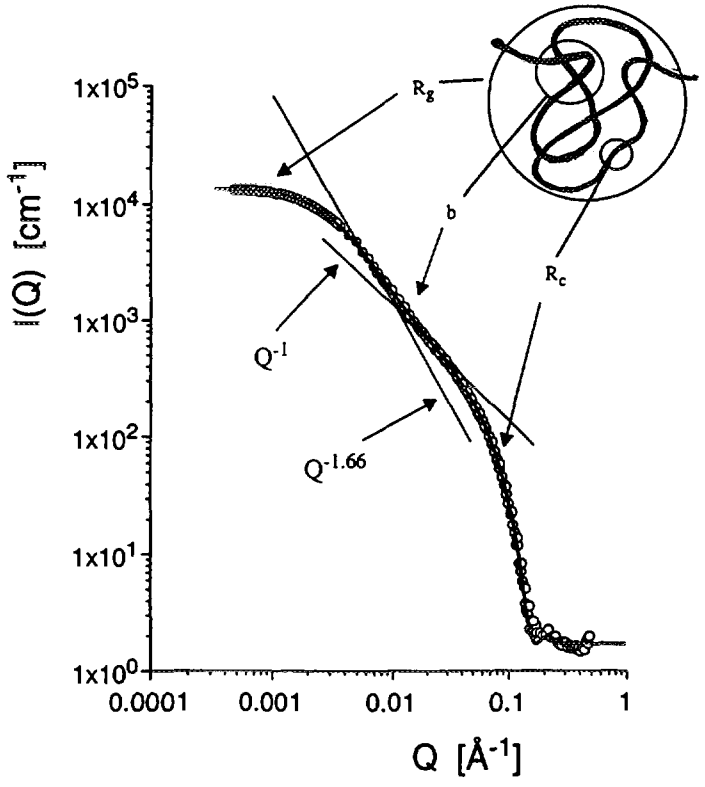

Fig. 6: Plot of scattering intensity $I(q)$ versus scattering vector q for solutions of soybean lecithin in deuterated isooctane (water-to-lecithin molar ratio w_o = 1.5) at volume fraction ϕ = 0.0021. Data shown is obtained from light (Δ) and neutron (O) scattering experiments. Also indicated are the regimes/length scales where a different characteristic q-dependence can be observed (see text for details).

the locally cylindrical structure of these reverse micelles and an estimate of the persistence length and overall dimensions.[43, 44]

In most previous studies, the data analysis primarily relied on an interpretation of different Q-regimes based on asymptotic expressions such as a Guinier approximation or the Debye equation for the low-Q part, the use of simple crossover relations for the incorporation of flexibility in the intermediate Q-range or a Guinier approximation for the high-Q part.[30-33, 35] However, in order to fully take advantage of the information content of the data it is desirable to perform a least squares analysis employing a model cross section as given for example by Eq. 3 for semiflexible polymers in good solvents. This is important, for example, in any attempt to determine the micellar flexibility characterized by the Kuhn length b, which is a key parameter in the interpretation of the micellar properties within the flexible surface model.[10, 34] Fig. 6 demonstrates that the scattering function developed for the wormlike chain model with excluded volume effects is indeed capable of quantitatively reproducing the experimental features of the SANS data from polymerlike micelles over an extended range of scattering vectors.

In the analysis of the local structure we can not only use model scattering functions as given by Eqs. 3-5, but we can try to extract detailed information on the local scattering length density profile of the micelles using a model-independent approach. This can be achieved through the indirect Fourier transformation (IFT) and square-root deconvolution (SQDEC) methods.[34, 36-39] The high-Q part of the polymer-like scattering intensity reflects the local cylindrical symmetry of the micelles, and the cross-section scattering intensity at $Q = 0$, $I_c(0)$, is directly related to the mass per length M_L.[40] While IFT uses the assumption that the cross-sectional contribution to the total scattering can be decoupled from the rest, it has the advantage that it does not rely on the low-Q part of the data used in the model fitting approach and that no specific model assumptions have to be made regarding the structure of the micelles except for the locally cylindrical symmetry. Therefore contributions from polydispersity of the overall size and interaction effects are minimized, which should result in a more reliable determination of the local micellar structure in micellar samples at finite concentrations.

Here I present experimental results from a detailed small-angle neutron scattering study of polymer-like lecithin reverse micelles (for details see [41, 42]). SANS experiments with polymer-like lecithin reverse micelles in cyclohexane provide an ideal test for the applicability of IFT and SQDEC methods. In cyclohexane, the water-induced formation of giant cylindrical micelles occurs at relatively high values of the molar ratio water-to-lecithin, w_0, which according to the previously postulated model for the micellar structure should lead to a tubular arrangement with a well defined water core and a surfactant shell. One thus has the possibility to dramatically modify the cross-section excess scattering length density profile $\Delta\rho(r)$ by using deuterated cyclohexane as the solvent and either H_2O or D_2O. This is demonstrated in Fig. 7, where a schematic drawing of $\Delta\rho(r)$ versus the cross-section radius R_c is shown for $w_0 = 14$ and both H_2O as well as D_2O. From an application of the IFT and SQDEC methods to SANS data obtained on absolute scale, one should be able to resolve the corresponding variations in $\Delta r(r)$ and obtain quantitative agreement with the known scattering length densities of the water core and the lecithin headgroup and tail regions.

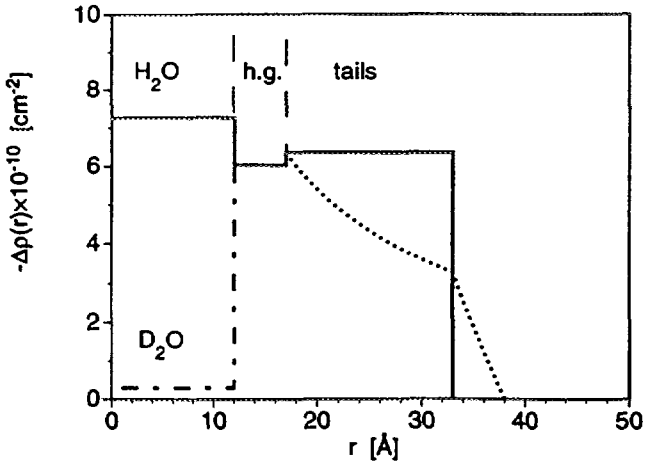

Fig.7: Schematic representation of the expected radial cross-section excess scattering length density profiles for lecithin reverse micelles in deuterated cyclohexane with a molar ratio of water to lecithin w_0 = 14 with either H_2O ($\Delta\rho^{H_2O}(r)$, solid line) or D_2O ($\Delta\rho^{D_2O}(r)$, dashed-dotted line) as based on a simple model of tubular aggregates with a well defined water core and surfactant shell. Also shown is the result of a simple geometrical model that includes solvent penetration into the tail region as the dotted line.

The results from measurements with lecithin reverse micelles in deuterated cyclohexane at $w_0 = 14$ and a lecithin concentration of C = 30 mM (which corresponds to a total (surfactant plus water) weight concentration of C_w = 30.6 mg/ml for w_0 = 14.0) are summarized in Fig. 8. We see from Fig. 8 that the exchange of H_2O with D_2O indeed results in a significant variation of the Q dependence of the scattering intensity I(Q). If H_2O is used, both water and lecithin have comparable scattering length densities. The expected radial cross-section excess scattering length density profile $\Delta\rho(r)$ can then be approximated by a simple step function modified by the solvent penetration into the chain region at higher values of r, which will cause a smoother decay of $\Delta\rho(r)$ (Fig. 7). This results in the typical monotonically decaying scattering pattern of a locally cylindrical particle with an intermediate Q^{-1} dependence of I(Q) followed by an exponential (Guinier) decay due to the cross-section form factor.[34] However, when D_2O is used instead of H_2O, the reduced excess scattering length density in the water core of the tubular reverse micelles results in a pronounced shell contrast (see Fig. 7), and a well defined first minimum of the cross-section form factor now becomes visible at high Q values. Having seen that the scattering data qualitatively agrees with our expectations based on the structural model of tubular reverse micelles, we can try to extract much more quantitative information on the local micellar structure by applying the indirect Fourier transformation (IFT) method to the experimental data.[36, 37] Starting point is again the decoupling approximation given by Eq. 3. Provided that $R_g > b > R_c$, for $bQ >> 1$ the high-Q asymptotic behavior can then be expressed by

$$I(Q) = \left(\frac{\pi}{Q}\right) 2\pi \int_0^\infty \tilde{p}_c(r)\, J_0(Qr)\, dr = \frac{\pi}{Q} I_c(Q) \qquad (6)$$

where the normalized cross-section distance distribution function $\tilde{p}_c(r)$ is given by

$$\tilde{p}_c(r) = \frac{2\pi C_w}{M_L} \int_0^\infty \Delta\rho(r')\, \Delta\rho(r + r')\, r'\, dr' \qquad (7)$$

and $J_0(x)$ is the zeroth order Bessel function. Note that $\tilde{p}_c(r)$ and $I_c(Q)$ contain a factor C_w/M_L, which is important for absolute normalization.

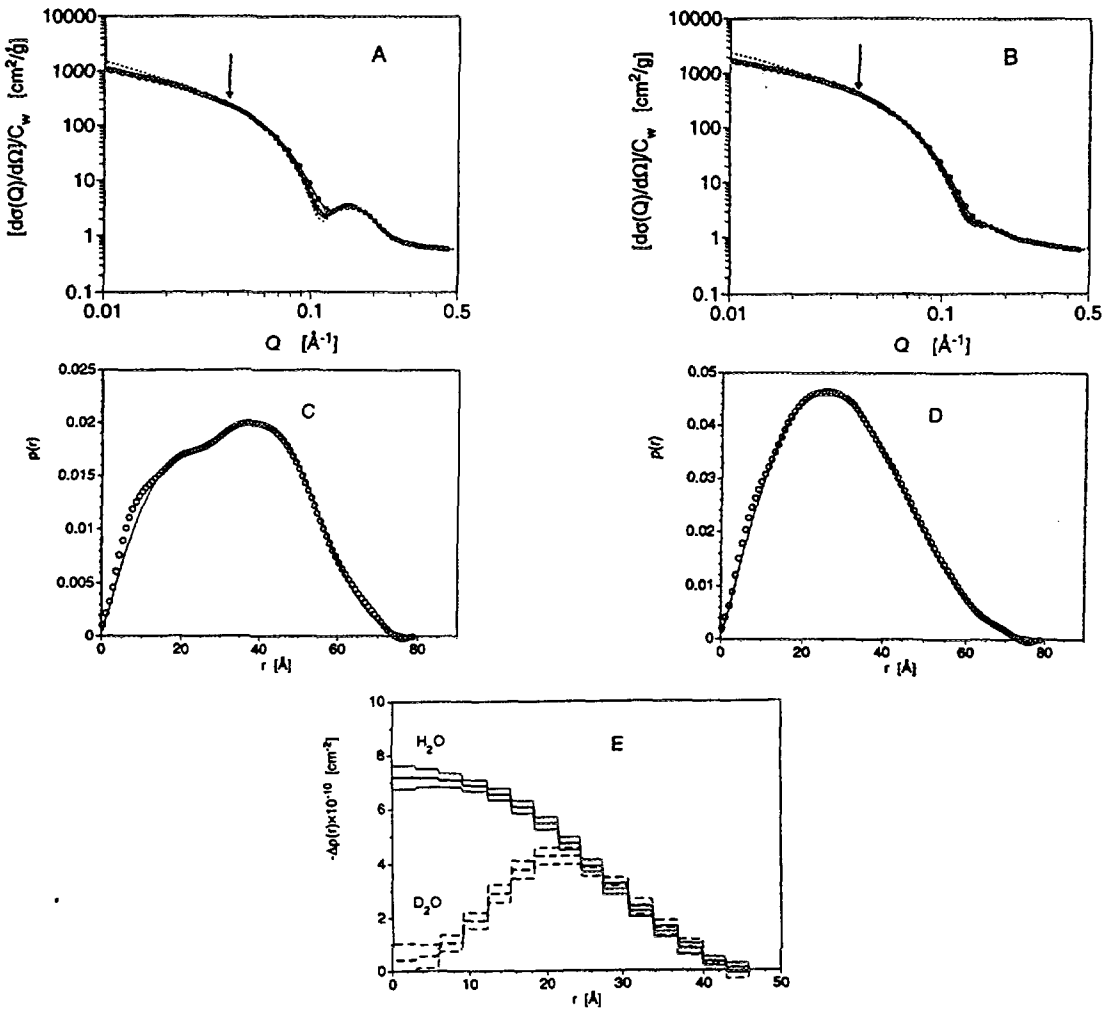

Fig. 8: A comparison of the experimental (o) and fitted (using the indirect Fourier transform method) normalized scattering intensity $[d\sigma(Q)/d\Omega]/C_w$ (A, B), the corresponding distance distribution functions $\tilde{p}_c(r)$ (C, D) and the radial cross-section excess scattering length density profiles (as obtained by the square-root deconvolution method) (E) for lecithin reverse micelles in deuterated cyclohexane at w_0 = 14.0: (A,B): $[d\sigma(q)/d\Omega]/C_w$ versus q for measurements with D_2O (A) and with H_2O (B). The solid lines correspond to the intensity smeared by the instrumental resolution, and the dotted line corresponds to the ideal intensity (Note that the data obtained with different combinations of neutron wavelenght and sample-detector distance and the corresponding fitted curves are slightly shifted due to resolution effects.). Also shown by the arrow is the lower cut-off value of the q range used for the IFT. (C, D): $\tilde{p}_c(r)$ versus r as determined by IFT for measurements with D_2O (C) and with H_2O (D), respectively. Also shown as the full curves are fits to the data by the square-root deconvolution procedure for $\tilde{p}_c(r)$, resulting in the radial cross-section excess scattering length density profile $\Delta\rho^{H_2O}(r)$ (solid line) or $\Delta\rho^{D_2O}(r)$ (dashed line) shown in (E). The light lines in (E) indicate the errors in $\Delta\rho(r)$.

We can deduce a parameterized form of $\tilde{p}_c(r)$ through the IFT method. The lower limit Q_{min} = 0.04 Å^{-1} of the fitted Q-range (indicated by the arrows in Fig. 8) was chosen in accordance with the known Kuhn length of b ≈ 240 Å.[32, 41] A very good fit of the experimental data can be achieved with the applied IFT method, and the thus

obtained $\tilde{p}_c(r)$ functions closely resemble the simulated functions for filled and hollow cylindrical particles (see for example Fig. 3 of ref. [41]). Furthermore, a well defined shoulder with an initially linear region below $r \leq 10$ Å is also clearly visible and is most likely due to so-called diffuse longitudinal correlations as described in detail in ref. [41] (see Fig. 14 B in ref. [41]). The $\tilde{p}_c(r)$ functions vanish both in the "homogeneous cylinder" (H_2O) as well as in the "shell" (D_2O) contrast at approximately 70 Å, thus qualitatively confirming the previously postulated geometrical model which would predict a cross-section radius $R_c \approx 30$ Å. Having determined $\tilde{p}_c(r)$, we can calculate the integral parameters of the micellar cross-section using the corresponding relations for the cross-section radius of gyration $R_{c,g}$

$$R_{c,g}^2 = \frac{\left(\int_0^\infty r^2 \tilde{p}_c(r)\, dr \right)}{\left(2 \int_0^\infty \tilde{p}_c(r) dr \right)} \tag{8}$$

the cross-section forward scattering intensity $I_c(0)$

$$I_c(0) = 2\pi \int_0^\infty \tilde{p}_c(r) dr \tag{9}$$

and the mass per unit length M_L in units g/cm given by

$$M_L = \frac{I_c(0)}{\Delta\rho\, m^2} \tag{10}$$

In addition to the evaluation of these integral parameters of the micellar cross-section, we can also aim at a quantitative estimate of the radial cross-section excess scattering length density profile $\Delta\rho(r)$ from the $\tilde{p}_c(r)$ functions using the SQDEC method as described in detail in ref. [41]. The resulting profiles $\Delta\rho(r)$ versus r in absolute units (cm^{-2}) as well as the agreement between $\tilde{p}_c(r)$ determined from IFT and fitted using SQDEC are also shown in Fig. 8 C-E. Except for the initial part of the $\tilde{p}_c(r)$ function, which is strongly influenced by diffuse longitudinal correlations and which therefore was not used in the fitting procedure, the fit using the SQDEC method results in good agreement. Moreover, the thus obtained excess scattering length density profiles $\Delta\rho(r)$ for H_2O and D_2O are in close agreement with the expectations based on the geometrical model and the known scattering length densities of lecithin and water. The clear difference in $\Delta\rho(r)$ at low values of r and the subsequent perfect overlap at higher values of r provides us with a first direct estimate of the extension of the water core. The values of approximately 20 Å for the extension of the water into the headgroup region and approximately 22 Å for the hydrophobic tail region are in good agreement with the geometrical dimensions of the lecithin molecule and the relative volumes of water, headgroup and tail region. Moreover, the entire data analysis has been performed in absolute units throughout, and no free parameters have been used to adjust the obtained $\Delta\rho(r)$ values such as to make them for example overlap in the tail region. The degree of overlap in the chain region between the data sets from samples with H_2O and D_2O is extremely good and provides us with a very sensitive test of the applied data normalization procedure. The cross-section excess scattering length density profiles given in Fig. 8 E provide us for the first time with a direct verification of the

previously postulated geometrical model of a tubular cross-section with a well defined water core and a surfactant shell for the structure of polymerlike lecithin reverse micelles.

3. Outlook

The preceding two sections have given a few selected examples on the application of SANS for a characterization of structural properties of soft condensed matter systems. These examples hopefully demonstrate how powerful a tool SANS can be in these areas, in particular when combined with contrast variation experiments and the application of suitable theoretical models. However, while these were quite classical examples of the application of SANS to soft condensed matter research, with the advent of more powerful SANS instruments with very high neutron flux and large two-dimensional detectors becoming available (such as for example D22 at ILL), new possibilities for experiments under non-equilibrium conditions and time-resolved studies of structural transitions and phase transitions become feasible.

4. Acknowledgement

These lecture notes have greatly benefited from contributions made by Carolina Cavaco, Stefan Egelhaaf, Götz Jerke, and Jan Skov Pedersen.

5. References

[1] P. G. de Gennes, *Scaling Concepts in Polymer Physics* (Ithaca, N.Y.: Cornell University Press, 1979)
[2] H. Fujita, *Polymer Solutions* (Amsterdam: Elsevier, 1990)
[3] H. Yamakawa, *Modern Theory of Polymer Solutions* (New York: Harper & Row, 1971); Vol. .
[4] R. Klein and B. D'Aguanno In *Light Scattering, Principles and development*; W. Brown, Ed. (Oxford: Clarendon Press, 1996); pp 30.
[5] R. J. Hunter, *Foundations of Colloid Science* (Oxford: Clarendon Press, 1986)
[6] J. N. Israelachvili, *Intermolecular and Surfaces Forces;* 2 ed. (London: Academic Press, 1992)
[7] D. F. Evans and H. Wennerström, *The Colloidal Domain: Where Physics, Chemistry, Biology and Technology Meet* (New York: VCH Publishers Inc., 1994)
[8] S. A. Safran In *Structure and dynamics of strongly interacting colloids and supramolecular aggregates in solution*; S. H. Chen, J. S. Huang and P. Tartaglia, Ed. (Dordrecht: Kluwer Academic Publishers, 1992); Vol. 369; pp 237.
[9] M. Rawiso, R. Duplessix and C. Picot, *Macromolecules* **20** (1987) 630.
[10] J. S. Pedersen and P. Schurtenberger, *Macromolecules (submitted)* (1996)
[11] J. S. Pedersen, M. Laso and P. Schurtenberger, *submitted to Phys. Rev. E* (1996)
[12] T. Yoshizaki and H. Yamakawa, *Macromolecules* **13** (1980) 1518.
[13] H. Utiyama, Y. Tsunashima and M. Kurata, *J. Chem. Phys.* **55** (1971) 3133.
[14] T. Neugebauer, *Ann. Phys. (Leipzig)* **42** (1943) 509.
[15] D. Langevin, *Annu. Rev. Phys. Chem.* **43** (1992) 341.
[16] U. Olsson and Wennerström, *Adv. Colloid Interface Sci.* **49** (1994) 113.
[17] D. F. Evans, D. J. Mitchell and B. W. Ninham, *J. Phys. Chem.* **90** (1986) 2817.

[18] M. E. Cates and S. J. Candau, *J. Phys.: Condens. Matter* **2** (1990) 6869.
[19] G. Porte, J. Marignan, P. Bassereau and R. May, *J.Phys.France* **49** (1988) 511.
[20] U. Olsson and P. Schurtenberger, *Langmuir* **9** (1993) 3389.
[21] J. N. Israelachvili, D. J. Mitchell and B. W. Ninham, *J.Chem.Soc.Farad.Trans.II* **72** (1976) 1525.
[22] B. Lindman, U. Olsson, H. Wennerström and P. Stilbs, *Langmuir* **9** (1993) 625.
[23] D. Anderson, H. Wennerström and U. Olsson, *J. Phys. Chem.* **93** (1989) 4243.
[24] M. S. Leaver, U. Olsson, H. Wennerström and R. Strey, *J. Phys. II* **4** (1994) 515.
[25] M. Leaver and U. Olsson, *Langmuir* **10** (1994) 3449.
[26] P. Schurtenberger and C. Cavaco, *J. Phys. Chem* **98** (1994) 5481.
[27] T.-L. Lin, S.-H. Chen, N. E. Gabriel and M. F. Roberts, *J. Phys. Chem.* **91** (1987) 406.
[28] R. P. Hjelm, P. Thiyagarajan and H. Alkan, *J.Appl.Cryst.* **21** (1988) 858.
[29] R. P. Hjelm, P. Thiyagarajan, D. S. Sivia, P. Lindner, H. Alkan and D. Schwahn, *Progr.Colloid.Polym.Sci.* **81** (1990) 225.
[30] R. P. Hjelm, P. Thiyagarajan and H. Alkan-Onyuksel, *J.Phys.Chem.* **96** (1992) 8653.
[31] P. Schurtenberger, R. Scartazzini, L. J. Magid, M. E. Leser and P. L. Luisi, *J. Phys. Chem.* **94** (1990) 3695.
[32] P. Schurtenberger, L. J. Magid, S. King and P. Lindner, *J.Phys.Chem.* **95** (1991) 4173.
[33] M. A. Long, E. W. Kaler, S. P. Lee and G. D. Wignall, *J. Phys. Chem.* **98** (1994) 4402.
[34] J. S. Pedersen, S. U. Egelhaaf and P. Schurtenberger, *J. Phys. Chem.* **99** (1995) 1299.
[35] J. Marignan, J. Appell, P. Bassereau, G. Porte and R. P. May, *J. Phys. France* **50** (1989) 3553.
[36] O. Glatter, *J. Appl. Cryst.* **10** (1977) 415.
[37] O. Glatter, *J. Appl. Cryst.* **13** (1980) 577.
[38] O. Glatter, *J. Appl. Cryst.* **14** (1981) 101.
[39] O. Glatter and B. Hainisch, *J. Appl. Cryst.* **17** (1984) 435.
[40] O. Glatter In *International Tables for Crystallography*; A. J. C. Wilson, Ed. (Dordrecht: Kluwer Academic Publishers, 1992); Vol. C; pp 89.
[41] J. S. Pedersen and P. Schurtenberger, *J. Appl. Cryst.* (in press)
[42] P. Schurtenberger, G. Jerke, C. Cavaco and J. S. Pedersen, *Langmuir* **12** (1996) 2433.
[43] P. Schurtenberger, L. J. Magid, S. M. King and P. Lindner, *J.Phys.Chem.* **95** (1991) 4173.
[44] P. Schurtenberger, L. J. Magid, P. Lindner and P. L. Luisi, *Prog. Colloid Polym. Sci.* **89** (1992) 274.